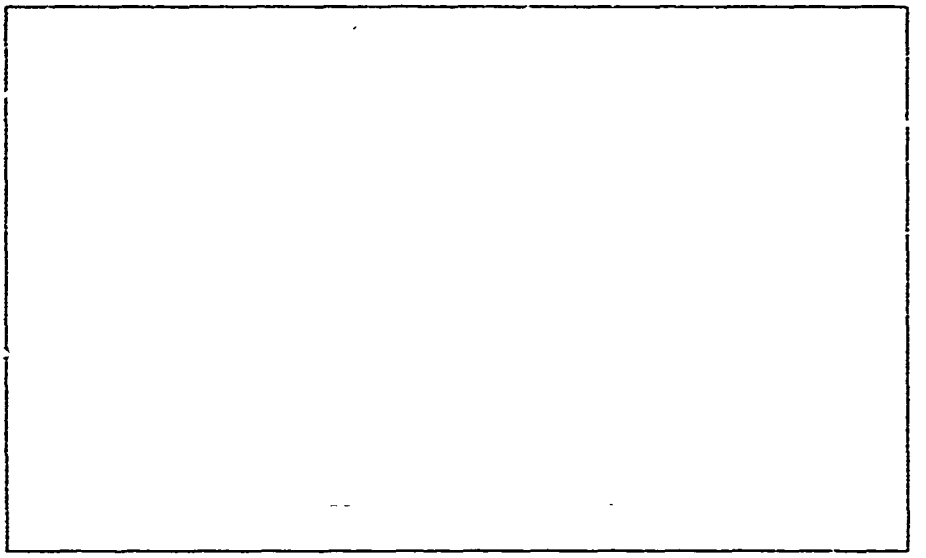

drexel university

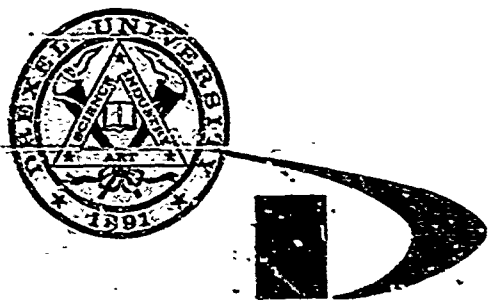

unclassified

Security Classification

DOCUMENT CONTROL DATA - R & D

(Security classification of title, body of abstract and indexing annotation must be entered when the overall report is classified)

1. ORIGINATING ACTIVITY (Corporate author)	2a. REPORT SECURITY CLASSIFICATION
Drexel University Philadelphia, Pennsylvania 19104 Department of Metallurgical Engineering	unclassified
	2b. GROUP

3. REPORT TITLE

A STRUCTURAL STABILITY-MECHANICAL BEHAVIOR CORRELATION IN EUTECTIC Al-$CuAl_2$
(The Role of the Interface on the Mechanical Behavior of Metal-Matrix Composites)

4. DESCRIPTIVE NOTES (Type of report and inclusive dates)

Technical Report

5. AUTHOR(S) (First name, middle initial, last name)

A. Pattnaik and A. Lawley

6. REPORT DATE	7a. TOTAL NO OF PAGES	7b. NO OF REFS
April 1972	33	33

8a. CONTRACT OR GRANT NO	9a. ORIGINATOR'S REPORT NUMBER(S)
ONR #N00014-67-A-0406-0001	Research Project #336 Technical Report #8
b. PROJECT NO. NR.031-721/2-10-67	
c.	9b. OTHER REPORT NO(S) (Any other numbers that may be assigned this report)
d.	

10. DISTRIBUTION STATEMENT

Reproduction in whole or part is permitted for any purpose of the United States Government. Distribution of this document is unlimited.

11. SUPPLEMENTARY NOTES	12. SPONSORING MILITARY ACTIVITY
Details of illustrations in this document may be better studied on microfiche	Office of Naval Research Metallurgy Branch Arlington, Virginia

13. ABSTRACT

Ambient temperature tensile yielding, flow, and fracture behavior have been correlated with interface microstructure, matrix substructure and fracture morphology in lamellar Al-$CuAl_2$ of small lamellar spacing (~2μ). To examine structural stability, and the effect of structural change on deformation behavior, composites were subjected to temperatures in the range $0.93T_{Eutectic}$ to $0.98T_{Eutectic}$ for periods up to 100 hours prior to testing.

Elevated temperature exposure does not cause any significant changes in stage I modulus, tensile yield point at the end of stage I, tensile strength or fracture behavior. Linear work-hardening of the composite in stage II is observed after elevated temperature exposure but not in the directionally solidified condition. Physicochemical instability is reflected in a coarsening of the microstructure and faceting of the $CuAl_2$ intermetallic; the lamellae remain aligned in the growth direction.

Tensile strength in the directionally solidified condition can be predicted from the rule-of-mixtures provided the true 'in-situ' flow stress of the aluminum solid solution and an 'effective' volume fraction for the reinforcing phase $CuAl_2$ are used. (over).

DD FORM 1 NOV 65 1473 (PAGE 1)

S/N 0101-807-6801

unclassified

Security Classification

14. KEY WORDS	LINK A		LINK B		LINK C	
	ROLE	WT	ROLE	WT	ROLE	WT
eutectic alloys						
interfaces						
structure						
crystallography						
stability						
mechanical-properties						

(Abstract, continued)

Differences in the work-hardening behavior are attributed to differing initial and deformation substructures of the ductile phase in the directionally solidified condition and following elevated temperature exposure. Premature transverse cleavage of $CuAl_2$ lamellae produces microvoids which then coalesce due to shear or tensile failure of the ductile phase adjacent to the broken lamellae.

A STRUCTURAL STABILITY-MECHANICAL BEHAVIOR CORRELATION IN EUTECTIC Al-$CuAl_2$

A. Pattnaik and A. Lawley

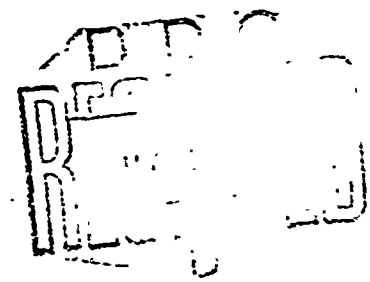

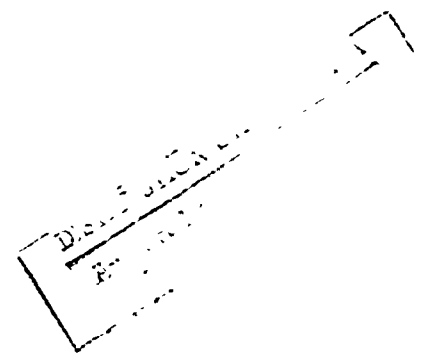

April 1972

Technical Report #8
Office of Naval Research
Arlington, Va.

Contract #N00014-67-A-0406-0001
(THE ROLE OF THE INTERFACE ON THE
MECHANICAL BEHAVIOR OF METAL-MATRIX COMPOSITES)

Drexel University
Department of Metallurgical Engineering
Philadelphia, Pennsylvania 19104

ABSTRACT

Ambient temperature tensile yielding, flow, and fracture behavior have been correlated with interface microstructure, matrix substructure and fracture morphology in lamellar Al-$CuAl_2$ of small lamellar spacing ($\sim 2\mu$). To examine structural stability, and the effect of structural change on deformation behavior, composites were subjected to temperatures in the range $0.93T_{Eutectic}$ to $0.98T_{Eutectic}$ for periods up to 100 hours prior to testing.

Elevated temperature exposure does not cause any significant changes in stage I modulus, tensile yield point at the end of stage I, tensile strength or fracture behavior. Linear work-hardening of the composite in stage II is observed after elevated temperature exposure but not in the directionally solidified condition. Physicochemical instability is reflected in a coarsening of the microstructure and faceting of the $CuAl_2$ intermetallic; the lamellae remain aligned in the growth direction.

Tensile strength in the directionally solidified condition can be predicted from the rule-of-mixtures provided the true 'in-situ' flow stress of the aluminum solid solution and an 'effective' volume fraction for the reinforcing phase $CuAl_2$ are used. Differences in the work-hardening behavior are attributed to differing initial and deformation substructures of the ductile phase in the directionally solidified condition and following elevated temperature exposure. Premature transverse cleavage of $CuAl_2$ lamellae produces microvoids which then coalesce due to shear or tensile failure of the ductile phase adjacent to the broken lamellae.

CONTENTS

		Page
I.	INTRODUCTION	1
II.	EXPERIMENTAL PROCEDURE	2
	A. Growth of Eutectic Composites	2
	B. Elevated Temperature Exposure	2
	C. Mechanical Testing	3
	D. Metallography	3
III.	EXPERIMENTAL OBSERVATIONS	4
	A. Tensile Behavior	4
	B. Composite Structure	5
	(i) Directionally Solidified Condition	5
	(ii) Following Elevated Temperature Exposure	5
	(iii) Deformation Substructure	6
	C. Fracture Morphology	7
IV.	DISCUSSION	9
	A. Composite Properties in the Directionally Solidified Condition	9
	(i) Stage II Behavior	9
	(ii) Strength Level	10
	B. Mechanical Behavior Following Elevated Temperature Exposure	11
	C. Interface Structure and Stability	13
	D. Fracture Mode	14
V.	SUMMARY AND CONCLUSIONS	15
VI.	REFERENCES	17
TABLES AND FIGURES		

I. INTRODUCTION

Since the phases of a directionally solidified eutectic composite are essentially in chemical equilibrium, the microstructure should be stable at elevated temperatures.[1] Observations on a number of systems attest to the generality of this phenomenon; thermal stability has been demonstrated in Al-$CuAl_2$,[2,3] Al-Al_3Ni,[4-10] Ni-Ni_3Nb,[11] Ni-Ni_3Ti,[12] CoAl-Co,[13] Cd-Zn,[14] and Fe-Cr-Nb.[15] However, eutectic composites are characterized by a large total interfacial area which may promote physicochemical instability.[4,16] The total interfacial energy per unit volume can be reduced by coarsening of the structure, by the growth of existing lower-energy interfaces at the expence of existing higher-energy interfaces, or by the formation of new lower-energy interfaces at the expence of existing interfaces.[4] Physicochemical instability is most pronounced at temperatures $\gtrsim 0.9\ T_{Eutectic}$ but the coarsening of the structure does not lead to significant changes in either the composition or amount of each phase in the composite.

In the present study, attention is directed to the effects of physicochemical instability and the associated structural changes on the ambient temperature mechanical behavior of lamellar Al-$CuAl_2$. A detailed correlation is made of tensile yielding, flow, and fracture with interface microstructure, matrix substructure and fracture morphology. Previously, Graham and Kraft[3] monitored the crystallography and kinetics of the coarsening process in this composite by means of x-ray diffraction and quantitative optical metallography.

Takahashi and Ashinuma[17] made in-situ observations on electron-transparent foils of Al-$CuAl_2$ at temperatures up to the eutectic (548°C). Butcher et al[18] attributed the spheroidization of the lamellar structure under stress at elevated temperature (300°C and 500°C) to a combination of diffusion and plastic flow. The possible relationships between coarsening and changes in mechanical behavior have not been examined.

II. EXPERIMENTAL PROCEDURE

A. Growth of Eutectic Composites:

Eutectic alloys were prepared from high-purity aluminum and copper. Homogenization and directional solidification were carried out in a vertical graphite crucible (induction heating) under a dynamic argon atmosphere. Growth rates in the range 7-11cm per hour gave a lamellar structure (spacing $\leq 2\mu$) with two or three grains in the 0.5in. dia. cross-section.

B. Elevated Temperature Exposure:

To assess elevated temperature structural stability, the as-grown composites in the form of tensile specimens (section C) were subjected to temperatures of 490°C, 510°C, or 530°C for times in the range 10-100 hours in a dynamic argon atmosphere. Since $T_{Eutectic}$ is 548°C, these correspond to homologous temperatures of $0.93T_E$, $0.95T_E$, and $0.98T_E$ respectively. After exposure, specimens were furnace-cooled to ambient temperature in order to minimize residual stresses, and to avoid any solution-treatment of the aluminum solid solution phase.

C. Mechanical Testing:

Two flat slabs (1.75" x 0.35" x 0.09") were cut from each ingot by means of a water-cooled diamond slitting wheel. Tensile specimens (gauge length 0.5", width 0.24", thickness ~0.09", shoulder radius 0.5") were then ground from the slabs using a contoured wheel. After electropolishing, SR-4 strain gauges were attached to the broad-faces of the gauge section. Tensile tests were performed in a standard Instron machine at a cross-head speed of 0.002" $min.^{-1}$ The dynamic modulus of the composite was determined by the resonance technique.[19]

D. Metallography:

Composite structures were characterized before and after tensile deformation in the directionally solidified condition and following elevated temperature exposure. A combination of optical metallography, electron fractography, transmission electron microscopy (TEM) and scanning electron microscopy (SEM) was utilized.

Following standard procedures including vibratory polishing, specimens for optical metallography were etched in Keller's reagent which darkens the $CuAl_2$ phase. In order to delineate cracks in the $CuAl_2$ phase, it was necessary to etch in a solution of 5 drops of HF, 10 drops of HNO_3, 3ml. lactic acid and 80ml. water.[20] No surface preparation was required for the examination of fracture surfaces in the SEM (JSM-2). Ordinarily fractures were viewed in the secondary electron image mode. In light of the limiting resolution of the SEM (~200°A), it was found to be advantageous to prepare replicas from fracture surfaces of composites in the directionally solidified condition. A two-stage technique was followed which gave a final surface replica of

silicon monoxide shadowed with germanium.[21]

For TEM (JEM-120) slices ~0.090" x ~0.090" x ~0.040" were cut from the composite with a diamond slitting wheel. Cuts were oriented relative to the growth direction to give transverse sections (perpendicular to the direction of growth) or longitudinal sections (parallel to the direction of growth). Electron-transparent specimens were then prepared from each slice by means of a combined jet-polishing and final thinning sequence.[22] Typically, electron-transparent areas were ~0.10" from the actual fracture surface.

III. EXPERIMENTAL OBSERVATIONS

A. Tensile Behavior:

Representative engineering stress-strain curves for lamellar composites grown at 9cm per hour are illustrated in figure 1. No necking was observed prior to fracture. From the dynamic resonance measurements and the initial slope of each stress-strain curve, it is concluded that Young's modulus is not affected by prior elevated temperature exposure.

In the directionally solidified condition, there is a gradual transition from stage I (in which the aluminum rich solid solution phase (α) and the $CuAl_2$(θ) intermetallic both deform elastically) to stage II (θ still elastic but the α phase plastic). Work-hardening of the composite is a function of strain. In contrast, stress-strain curves after elevated-temperature exposure were always found to give a distinct change in slope at the end of stage I, and a work-hardening rate in stage II that is independent of strain.

Tensile properties of the lamellar composites, with or without prior elevated temperature exposure, are summarized in table I. It is clear that the elevated temperature exposure has not brought about any significant decrease in yield and tensile strength or strain to fracture. This is both interesting and important in light of the accompanying coarsening of the lamellar structure, section B. The relative invariance of strength with exposure is further illustrated in figure 2.

B. Composite Structure:

(i) Directionally Solidified Condition

Optical micrographs of longitudinal and transverse sections are compared in figure 3. The lamellar or transverse faults TF in figure 3(b), and the longitudinal faults in figure 3(a) constitute a local breakdown of the lamellar structure due to variations in growth conditions. Typical TEM substructures in both planar and faulted regions of transverse sections are illustrated in figure 4. A detailed analysis of these faults, interface dislocations, and low angle grain boundaries has been made elsewhere.[22-25] Dislocations in the α phase in the vicinity of the interface are attributed to the presence of residual (thermal) stresses.[25]

(ii) Following Elevated Temperature Exposure

Structural changes accompanying elevated temperature exposure are shown in figure 5. The coarsening is initiated at faulted regions, figures 5(b) and 5(c). Though spheroidized after 100 hours at 530°C, longitudinal sections show that the structure remains aligned essentially parallel to the direction of growth, figure 6.

A more detailed picture of the coarsening processes is gained from the TEM study; representative micrographs following exposure at 530°C are shown in figures 7 and 8. These observations confirm that coarsening initiates at faulted regions such as terminal lamellae and show that the θ platelets recede from the original fault line with an accompanying thickening of adjacent θ platelets, figure 7(a). The preferred crystallography of the two phases is not altered during coarsening and low-angle tilt boundaries are preserved in order to maintain the original misorientations at the faults. In figure 7(c), the receding θ platelet carried the low-angle boundary along with it. After 100 hours at 530°C the structure spheroidizes and faceting of the θ phase is observed. Figures 8(a) and 8(b) compare the form of terminal lamellae before and after elevated temperature exposure. SEM of fracture surfaces confirms these microstructural features of the coarsened structure and also illustrates the increased contiguity of the θ intermetallic, section C.

The dislocation substructure in the α phase is relatively uniform, figure 7. However, in comparison to the directionally solidified condition (figure 4), the dislocation density is significantly higher (figure 7). This higher dislocation density following elevated temperature exposure is tentatively attributed to plastic flow of the α phase on slow cooling in order to relieve residual stress. There is no evidence of incoherent precipitation in the α phase.

(iii) Deformation Substructure

Representative micrographs of the deformation substructure in the α phase of transverse sections cut from directionally solidified composites tested to failure are illustrated in figure 9. Similar dislocation configurations are present in longitudinal sections.

Pattnaik and Lawley[25] observed this form of deformation substructure in the compressive loading of Al-$CuAl_2$.

Examples of the deformation substructure in composites tested to failure following elevated temperature exposure are given in figure 10. A uniformly high dislocation density is developed in the α-phase; this is in contrast to the pseudo-cell structure present in the α-phase of composites deformed in the directionally-solidified condition, figure 9. The interaction of glide dislocations in the α-phase with interfacial dislocations is seen in figures 10(b) and 10(c). Glide and interface dislocations could be differentiated by changing the conditions for diffraction contrast.

C. Fracture Morphology:

In tension, composite fracture surfaces are approximately perpendicular to the axis of loading. The microstructure in longitudinal sections close to the fracture surface is illustrated in figure 11.

Directionally solidified composites exhibit transverse cleavage of θ lamellae either at random or at a location of stress concentration e.g. adjacent to a broken θ platelet, figure 11(b). Crossman et al[20] have shown that cleavage of the θ lamellae begins in stage II and is due to a spectrum of strength levels of the lamellae. The density of broken lamellae as a result of premature cracking is not uniform throughout the composite; however, in the immediate vicinity of the fracture surface, broken lamellae are always seen, figure 11(a). Void coalescence then occurs either by matrix shear or by matrix necking, figure 11(a).

Elevated temperature exposure does not alter the mode of initiation or propagation of fracture, figure 11(c) and 11(d), although the incidence

of matrix shear between broken θ lamellae is rare. Cracking is observed at points of weakness in the coarsened structure, for example at cross-sectional minima in the θ platelets, figure 11(d).

Electron fractography and SEM confirm these structural characteristics of the fracture process. Representative electron fractographs (from two-stage replicas) of the composite in the directionally solidified condition are compared in figure 12. Transverse cleavage of θ platelets and necking of the α-phase to a knife edge is illustrated in figure 12(a). An example of transverse cleavage followed by shear of the α-phase is seen in figure 12(c). Cleavage steps on the θ phase can also be observed in some areas of the fracture surface, figure 12(b). The specific surface detail on the $CuAl_2$ phase is probably a function of the orientation of the θ platelets relative to the local path of fracture.

Fracture surfaces of the coarsened lamellar structure were amenable to direct observation in the SEM, figure 13. In figure 13(a) cleavage of the θ lamellae is accompanied by necking of the α-phase to a knife-edge profile; this micrograph also shows the prior recession of θ platelets from the original fault line. Coarsening leads to bridging of the θ lamellae and enhanced contiguity of the brittle intermetallic phase, figures 13(b) and 13(c). In this coarsened structure, the crack can propagate to adjacent lamellae via the bridges. Garmong and Rhodes[26] observe a similar mode of failure in the ternary Al-Cu-Mg eutectic composite; the brittle $CuMgAl_2$ intermetallic fails at weak points at low levels of strain.

IV. DISCUSSION

A. Composite Properties in the Directionally Solidified Condition:

(i) Stage II Behavior

On the basis of the rule-of-mixtures,[27] the slope of the stress-strain curve of the composite in stage II is given by:

$$E_c(II) = E_\theta V_\theta + \left(\frac{d\sigma}{d\varepsilon}\right)_\alpha (1 - V_\theta) \qquad (1)$$

where $E_c(II)$ is the secondary modulus of elasticity of the composite

E_θ is the Young's modulus of the θ intermetallic

V_θ is the volume fraction of the θ intermetallic

$\left(\frac{d\sigma}{d\varepsilon}\right)_\alpha$ is the slope of the α-phase (matrix) stress-strain curve in the uncombined state at the appropriate level of strain in stage II.

In the Al-$CuAl_2$ binary eutectic, $V_\theta = 0.475$ and E_θ has been determined[25] as 14.4×10^6 psi. The value of $(d\sigma/d\varepsilon)_\alpha$ is not precisely known but is $\sim 5 \times 10^4$ psi. Thus, $(d\sigma/d\varepsilon)_\alpha << E_\theta$ and equation (1) can be approximated to the form:

$$E_c(II) = E_\theta V_\theta \qquad (2)$$

The calculated value of $E_c(II)$ from equation (2) is 6.85×10^6 psi. However, at the initiation of stage II, the observed modulus (figure 1) is 5×10^6 psi. Since the error introduced by neglecting the second term in equation (1) is small, the discrepancy between the calculated and observed values of the secondary modulus $E_c(II)$ must reside in the parameter V_θ. Specifically, the result implies that the effective volume fraction of the reinforcing phase θ is lower than that calculated from the phase diagram.[20] Using the observed modulus (5×10^6 psi) in equation (2) and taking E_θ as 14.4×10^6 psi, the effective value of V_θ is 0.346; this is compared to the V_θ of 0.475 from the phase diagram.

In order to explain observed strength levels in the Ag-Ge eutectic composite, Krummheuer and Alexander[28] introduce the concept of an effective volume fraction for the reinforcing phase in stage II. The effective volume fraction is less than the actual volume fraction in stage II deformation since over the transfer length, the reinforcing phase is not able to carry as much load as the rest of the reinforcement length. In constrast, the transfer length in stage I is much smaller than in stage II so that V_θ(effective) = V_θ(actual).

(ii) Strength Level

Lamellar composites grown at a rate of 9cm per hour exhibit tensile strengths ~36,000 psi. The lower strengths obtained in composites grown at 11cm per hour (table I) are attributed to structural irregularities, primarily variations in the thickness of the θ platelets. This is probably a consequence of the inherent low value of the ratio 'temperature gradient at solid/liquid interface: solidification rate' in the crystal growing unit. Under the appropriate conditions for growth, and with the avoidance of major structural irregularities, the tensile strength of lamellar Al-$CuAl_2$ increases with increasing solidification rate.[29]

An accurate prediction of the tensile strength of the composite is possible from the rule-of-mixtures provided the effective volume fraction of the reinforcing phase and the true 'in-situ' flow stress of the α-phase matrix are known.

The form of the rule-of-mixtures equation is then:

$$\sigma_c(\text{UTS}) = \sigma_\theta(\text{UTS})\ V_\theta(\text{Eff}) + \sigma_\alpha^*(1 - V_\theta(\text{Eff})) \qquad (3)$$

where σ_c(UTS) is the ultimate tensile strength of the composite.

σ_θ is the strength of the $CuAl_2$ intermetallic at the fracture strain of the composite.

V_θ(Eff) is the effective volume fraction of the $CuAl_2$.

σ_α^* is the 'in-situ' flow stress of the matrix at the fracture strain of the composite.

From a comparison of the tensile and compressive behavior of Al-$CuAl_2$, and taking account of residual stresses, Pattnaik and Lawley[25] have shown that σ_α^* is~13,500 psi. Assuming elastic behavior of the θ phase to failure, with a measured failure strain ε_f of 0.55 (table I), $\sigma_\theta (= E_\theta \varepsilon_f)$ is 80,000 psi. Using V_θ(Eff) = 0.346 from the previous section, equation (3) gives a composite tensile strength of 36,400 psi. This is in good agreement with the measured strength of composites in the directionally solidified condition grown at 9cm per hour, table I.

B. Mechanical Behavior Following Elevated Temperature Exposure:

A comparison of the stress-strain curves in figure 1 leads to the following conclusions: (i) Young's modulus (stage I) and the stress level at the end of stage I (i.e. the composite yield point) are not affected by the prior elevated temperature exposure; (ii) the work-hardening slope in stage II is a function of strain, cf., the directionally solidified condition; (iii) high temperature exposure does not have a significant effect on tensile strength, figure 1 and table I.

Retention of ambient temperature strength following elevated temperature exposure has been reported in Nb-Nb_2C[30] and Al-Al_3Ni.[4] In the latter rod-like structure, exposure conditions (96 hours at 0.96 T_E) were similar to those selected in the present study. Notwithstanding the difference in the scale of the microstructure before and after exposure (figures 3, 5, and 6), the

coarsened structure remains aligned essentially parallel to the growth direction and there is no change in the relative proportions of each phase. It must, therefore, be concluded that in the coarsened condition the integrity of the interface is preserved and efficient load transfer to the reinforcing phase is possible.

Differences in work-hardening behavior in stage II between directionally solidified composites and those subjected to elevated temperature exposure can be discussed qualitatively in terms of equation (1). For $E_c(II)$ to vary with strain either $(d\sigma/d\varepsilon)_\alpha$ or V_θ must be strain dependent, where V_θ is the effective volume fraction of the θ phase. Of these possibilities it is considered that the matrix phase α is responsible and that $V_\theta(Eff)$ is relatively independent of strain up to fracture. The reasoning is as follows: After 10 hours exposure at 490°C, the composite microstructure is indistinguishable from that in the directionally solidified condition. Yet this exposure gives rise to a constancy of $(d\sigma/d\varepsilon)_{comp.}$ with strain in stage II. The effect of the elevated temperature exposure followed by slow cooling is to modify the dislocation substructure in the α-phase; in turn this influences work-hardening behavior. Specifically, in comparison to the directionally solidified condition (figure 4), the dislocation density after exposure is significantly higher, figure 7. Control of work-hardening in stage II of the composite by the hardening characteristics of the α-phase is at variance with conclusions drawn by Hertzberg et al[31] on Al-$CuAl_2$. The slope of stage II was attributed to premature cracking of the θ phase with a subsequent inequality of strains in the α and θ phases.[31]

The increase in interlamellar spacing due to elevated temperature exposure is expected to decrease the 'in-situ' strength of the α-phase.[25]

Since the average thickness of the θ lamellae also increases, the strength of the θ phase may be expected to decrease. Retention of ambient temperature strength (figure 1, table I) must therefore reflect an increase in the flow stress of the α phase σ_α^*. This is consistent with the observed high dislocation density in the undeformed α phase following elevated temperature exposure. In a similar manner, the increase in strength of Al-Al_3Ni with cold rolling was attributed to an increase in the flow stress of the aluminum solid solution phase.[5]

C. Interface Structure and Stability:

In the directionally solidified condition, deformation substructure of the α phase (figure 9) is similar to that for compressive loading.[25] The substructure approximates a cellular configuration but with a higher dislocation density at the interface than in the central regions of the α lamellae. Associated interface dislocation - glide dislocation interactions are expected to result in a high 'in-situ' yield stress of the α phase, as observed and discussed in the previous study of Al-$CuAl_2$ in compressive loading.[25] A value of 13500 psi for σ_α^* in equation (3) gave good agreement between predicted and measured composite strength; this 'in-situ' magnitude of σ_α^* is approximately three times higher than that of an unconstrained α solid solution.

Tensile deformation of composites given prior elevated temperature exposure results in a high but relatively uniform dislocation density across the α lamellae. The presence of interfacial dislocations in the coarsened structure (figures 10(b) and 10(c)) shows that semi-coherency is not destroyed. These micrographs provide further proof of interaction between glide dislocations in the α phase and 'misfit' dislocations at the

interface between the α and θ phases. As discussed in the previous section, the difference in substructure (before and after deformation) between the directionally solidified condition and that following elevated temperature exposure, is believed to be responsible for differences in work-hardening behavior in stage II.

In comparison with other studies on Al-$CuAl_2$,[2,3] the results of this investigation show that coarsening proceeded more rapidly. This is attributed to the smaller interlamellar spacing (≤2μ as compared to spacings in the range 5μ to 8μ) and therefore larger interphase area in our composites. In addition, the density of faulting tends to increase with decreasing spacing and this enhances coarsening. Prolonged high temperature exposure leads to faceting of the θ phase, figure 8(b). Since faceting results from the anisotropic nature of interfacial energy, it is clear that the interfaces present in the directionally solidified condition are not necessarily those of minimum energy. Basically, this means that the excellent thermal stability of eutectic composites cannot be attributed to the presence of special low-energy interphase interfaces. Similar conclusions have been drawn by Jaffrey and Chadwick[9] for coarsening in the rod-like Al-Al_3Ni eutectic composite.

D. Fracture Mode:

The mode of fracture of Al-$CuAl_2$ is similar in the directionally solidified condition and following elevated temperature exposure. In stage II deformation, premature cracking of θ platelets leads to localized void formation. Cracks also appear in adjacent θ lamellae due to stress concentrations. Void coalescence to macrocracks involves shear of the α phase or tensile necking of the α phase between θ lamellae, figure 11(a). Propagation of the unstable crack is followed by necking of the α phase to a knife edge, figure 12(a).

Similar surface structures have been reported by Gerberich[32] in the fracture of notched aluminum-stainless steel composites. Premature cracking of θ lamellae is implicit in this form of failure mode.[20,31] The observation of breaks in the θ platelets well away from fracture surfaces in this study is proof of this phenomenon; these have been shown to be a result of tensile deformation and are not present in the as-grown (directionally solidified) condition. Recent studies on the fracture of Al-$CuAl_2$ show that for high rates of solidification (~85cm per hour to 1000cm per hour) premature cracking does not occur.[29,33] This is attributed to 'whisker' behavior of the fine scale θ lamellae.

After elevated temperature exposure θ lamellae are interconnected by bridging (figure 13(b)), or by coalescence. Hence, a crack can propagate readily to neighboring lamellae through the θ phase. Optical metallography reveals the premature cracking of θ lamellae, figures 11(c) and 11(d). Cracking is observed at reduced cross sectional areas of θ lamellae, figure 11(d), however the total number of cracks in a given area is similar to that after deformation in the directionally solidified condition.

V. SUMMARY AND CONCLUSIONS

1. Elevated temperature exposure of Al-$CuAl_2$ (490°C to 530°C for periods up to 100 hours) does not cause any significant change in stage I modulus, tensile yield point at the end of stage I, or tensile strength.

2. Linear work hardening of the composite to fracture in stage II is observed after elevated temperature exposure. In contrast, work hardening is a function of strain in the directionally solidified condition.

3. Tensile strength in the directionally solidified condition can be predicted from the rule of mixtures if the 'in-situ' flow stress of the α phase and an effective volume fraction for the θ reinforcement are used.

4. Differences in work-hardening behavior are attributed to differing initial and deformation substructures in the α phase in the directionally solidified condition and following elevated temperature exposure.

5. Physicochemical instability is reflected in a coarsening of the microstructure but the lamellar structure remains aligned in the growth direction. Faceting of the θ phase is observed in the later stages of coarsening; it is concluded that interfaces in the directionally solidified composite are not necessarily those of minimum energy.

6. Tensile failure is not significantly altered by elevated temperature exposure. Premature transverse cleavage of θ lamellae produces microvoids. Shear or tensile failure of the α phase between broken θ lamellae cause void coalescence followed by the propagation of unstable cracks.

VI. REFERENCES

1. M. J. Salkind, Interfaces in Composites, ASTM Special Tech. Pub. #452, American Soc. Testing and Materials, p. 149 (1969).

2. R. W. Kraft, D. L. Albright, and J. A. Ford, Trans. TMS-AIME, vol. 227, p. 540 (1963).

3. L. D. Graham and R. W. Kraft, Trans. TMS-AIME, vol. 236, p. 94 (1966).

4. B. J. Bayles, J. A. Ford, and M. J. Salkind, Trans. TMS-AIME, vol. 239, p. 844 (1967).

5. M. Salkind, F. George, and W. Tice, Trans. TMS-AIME, vol. 245, p. 2339, (1969).

6. M. Salkind, G. Leverant, and F. George, J. Inst. Metals, vol. 95, p. 349 (1967).

7. S. Marich, Met. Trans., vol. 1, p. 2953 (1970).

8. H. B. Smartt, L. K. Tu, and T.H. Courtney, Met. Trans., vol. 2, p. 2717 (1971).

9. D. Jaffrey, and G. A. Chadwick, Met. Trans. vol 1, p. 3389 (1970).

10. Y. G. Nakagawa, and G. C. Weatherly, Acta Met., vol. 20, p. 345 (1972).

11. R. T. Quinn, R. W. Kraft, and R. W. Hertzberg, Trans. ASM, vol 62, p. 38 (1969).

12. K. D. Sheffler, R. W. Hertzberg, and R. W. Kraft, Trans. ASM, vol. 62, p. 105 (1969).

13. H. E. Cline, Trans. TMS-AIME, vol. 239, p. 1906 (1967).

14. B. Soutiere and H. W. Kerr, Trans., TMS-AIME, vol. 245, p. 2595 (1969).

15. D. Jaffrey and S. Marich, Met. Trans., vol. 3, p. 551 (1972).

16. N. Parratt, Chem. Eng. Prog., vol 62, p. 61 (1966).

17. N. Takahashi, and K. Ashinuma, J. Electron Microscopy, vol. 7, p. 37 (1960).

18. B. R. Butcher, G. C. Weatherly, and H. P. Pettit, Metal Sci. Journal, vol. 3, p. 7 (1969).

19. M. R. Pinnel, H. P. Cheskis, R. W. Heckel, and A. Lawley, Trans. TMS-AIME, vol. 245, p. 2119 (1969).

20. F. W. Crossman, A. S. Yue, and A. E. Vidoz, Trans. TMS-AIME, vol. 245 p. 397 (1969).

21. C. D. Beachem, in Fracture, an Advanced Treatise, Editor, H. Liebowitz, Academic Press, New York, vol. 1, p. 243 (1968).

22. G. C. Weatherly, Metal Sci. Journal, vol. 2, p. 25 (1968).

23. I. G. Davies and A. Hellawell, Phil. Mag. vol 19, p. 1285, (1969).

24. D. D. Double and A. Hellawell, Phil. Mag., vol. 19, p. 1229 (1969).

25. A. Pattnaik and A. Lawley, Met. Trans., vol. 2 p. 1529 (1971).

26. G. Garmong and C. G. Rhodes, Met. Trans., Vol. 3, p. 533 (1972).

27. D. L. McDanels, R. W. Jech, and J. W. Weeton, Trans. TMS-AIME, Vol. 233, p. 636 (1965).

28. W. R. Krummheuer and H. Alexander, Z. Metallkunde, Vol. 62, p. 129 (1971).

29. W. H. S. Lawson and H. W. Kerr, Met. Trans., Vol. 2, p. 2853 (1971).

30. F. D. Lemkey and M. J. Salkind, in Crystal Growth, Editor H. S. Peiser, Oxford University Press, p. 171 (1967).

31. R. W. Hertzberg, F. D. Lemkey, and J. A. Ford, Trans. TMS-AIME., Vol. 233 p. 342 (1965).

32. W. W. Gerbereich, J. Mech. Phys. Solids, Vol. 19, p. 71 (1971).

33. H. R. Bertorello and H. Biloni, Met. Trans., Vol. 3, p. 73 (1972).

TABLE I

Effect of Prior Elevated Temperature Exposure on the Ambient Temperature Tensile Strength of Al-$CuAl_2$ Lamellar Eutectic Composites

Solidification Rate (R) in (cm/hr)	Composite Condition	Yield Point (σ_c^Y) (psi)	Ultimate Tensile Strength (σ_c^{UTS}) (psi)	Strain to Fracture (e_f) (%)
7.0	As-grown	11,000	36,100	0.76
7.0	As-grown	11,000	34,000	0.60
9.0	As-grown	12,400	35,400	0.60
9.0	As-grown	12,000	37,600	0.50
9.0	530°C; 10 hrs.	11,000	26,600	0.46
9.0	530°C; 50 hrs.	8,000	27,400	0.465
9.0	530°C; 100 hrs.	10,000	32,800	0.51
9.0	490°C; 100 hrs.	6,000	26,200	0.44
9.0	510°C; 100 hrs.	11,000	35,200	0.55
11	As-grown	9,000	24,000	0.26
11	490°C; 100 hrs.	8,200	26,300	0.41
11	510°C; 100 hrs.	7,200	27,000	0.34
11	530°C; 100 hrs.	9,500	28,800	0.55

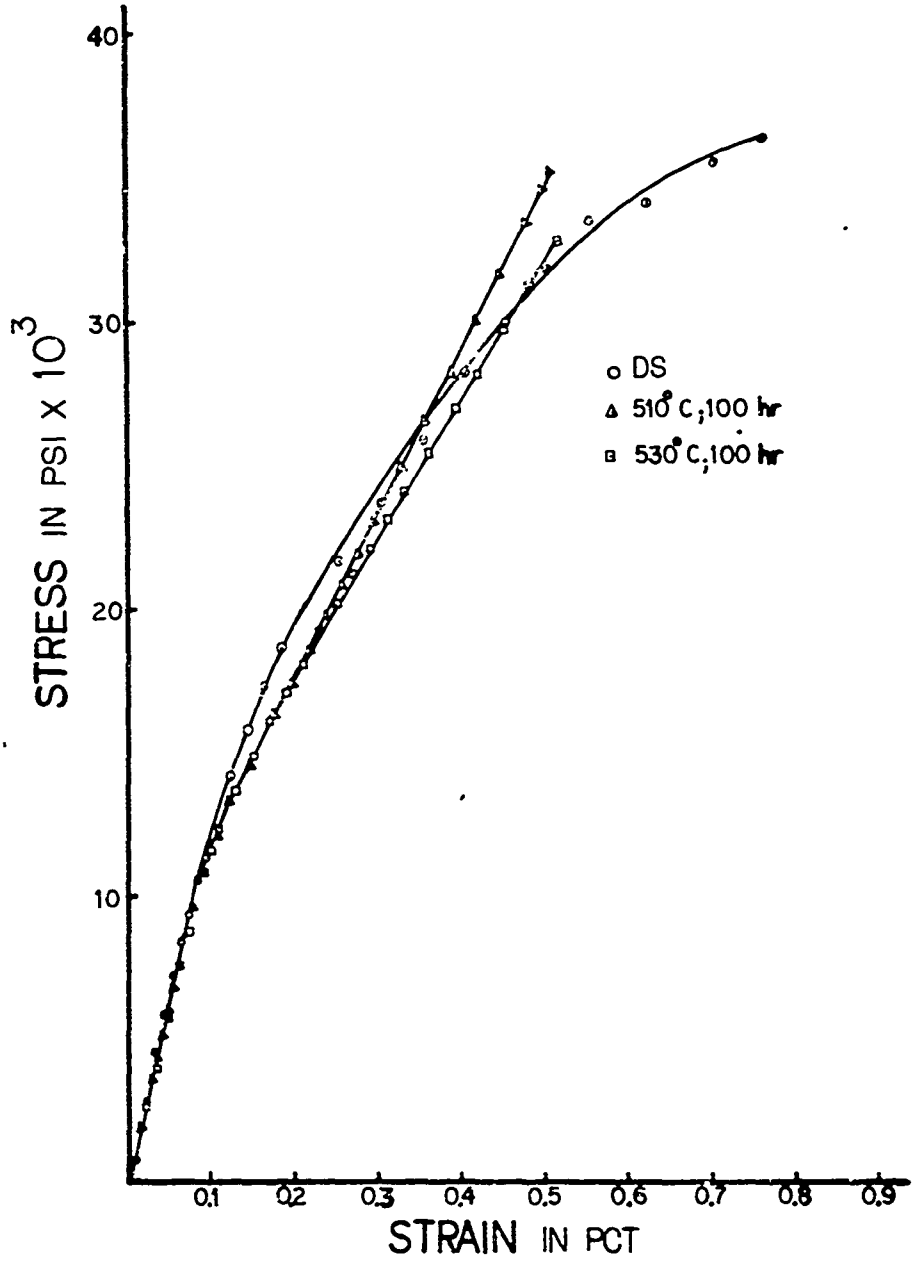

Figure 1

Representative tensile stress-strain curves for lamellar Al-$CuAl_2$ at room temperature in the directionally solidified condition (DS) and following elevated temperature exposure; growth rate 9cm per hour.

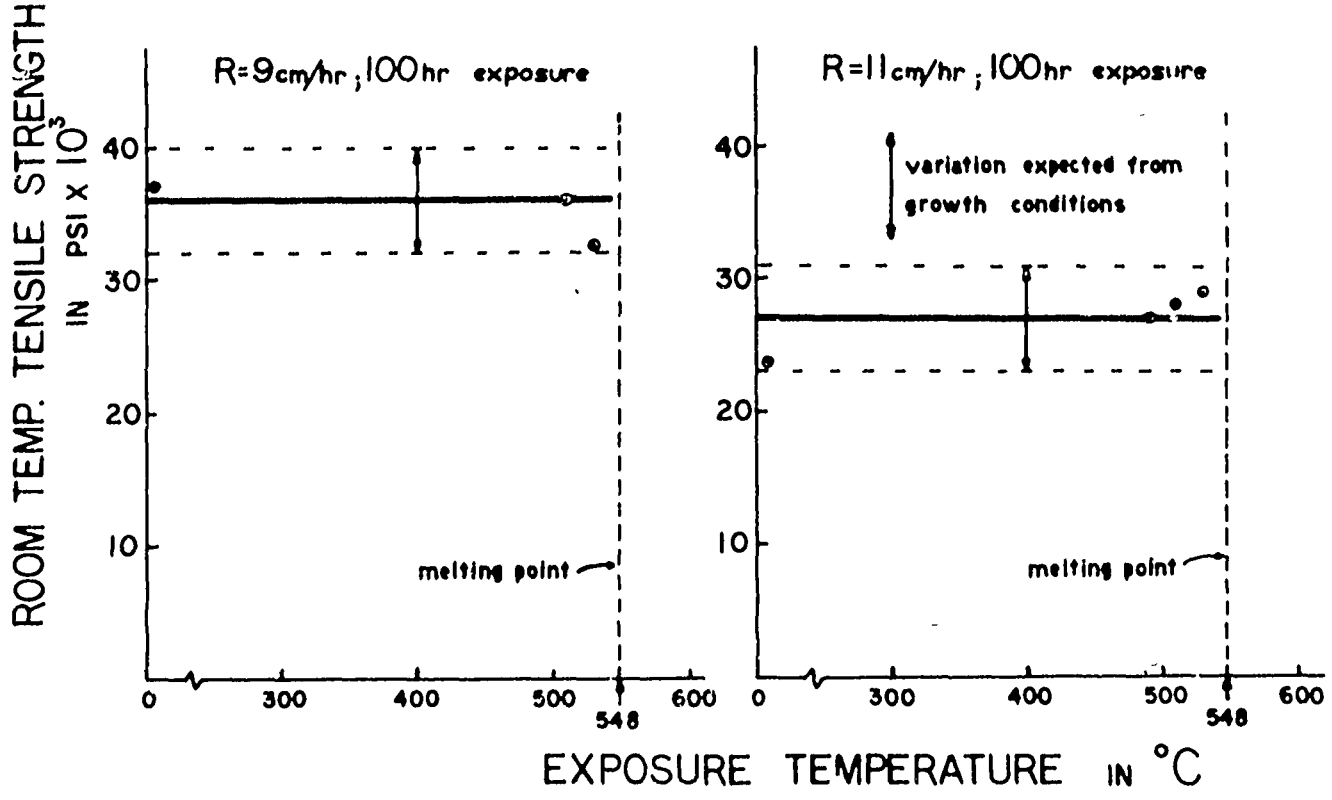

Figure 2

Effect of prior elevated temperature exposure on the room temperature tensile strength of lamellar eutectic Al-$CuAl_2$.

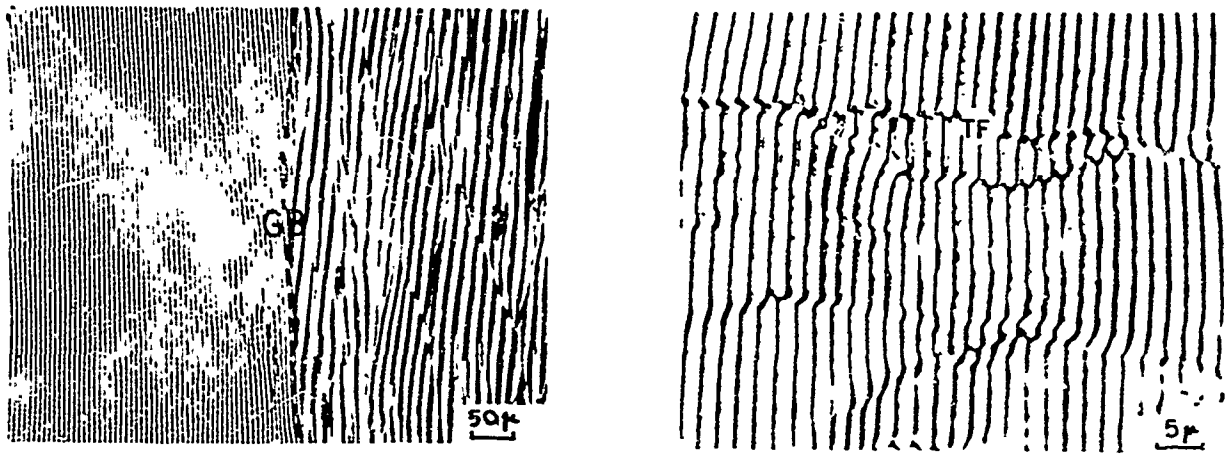

(a) (b)

Figure 3

Structure of directionally solidified composites grown at 9cm per hour - optical metallography (a) longitudinal section; GB = grain boundary; (b) transverse section; TF = transverse fault.

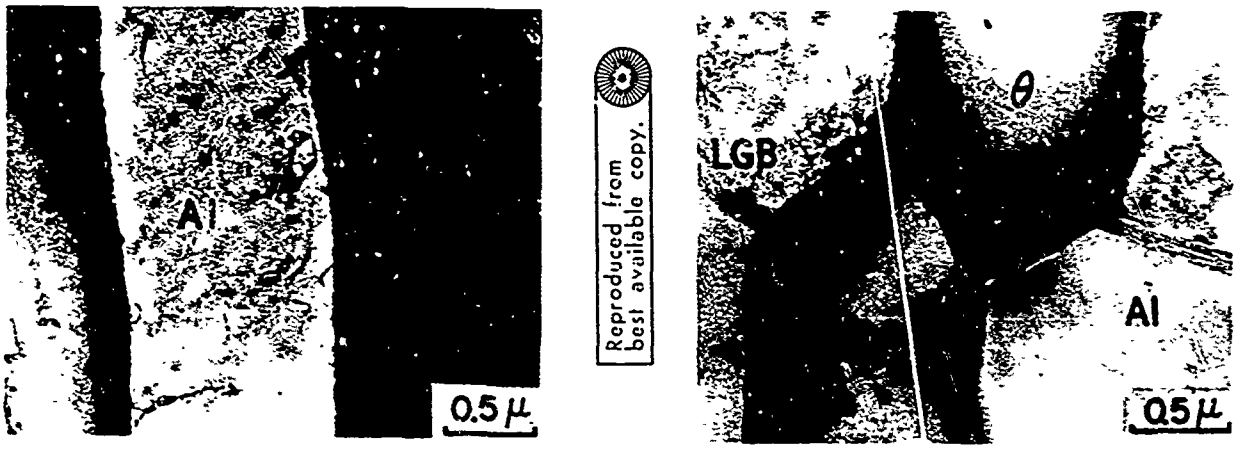

(a) (b)

Figure 4

Structure of directionally solidified composites grown at 9cm per hour - TEM (a) transverse section; (b) transverse section; LGB = low angle grain boundary, θ = $CuAl_2$.

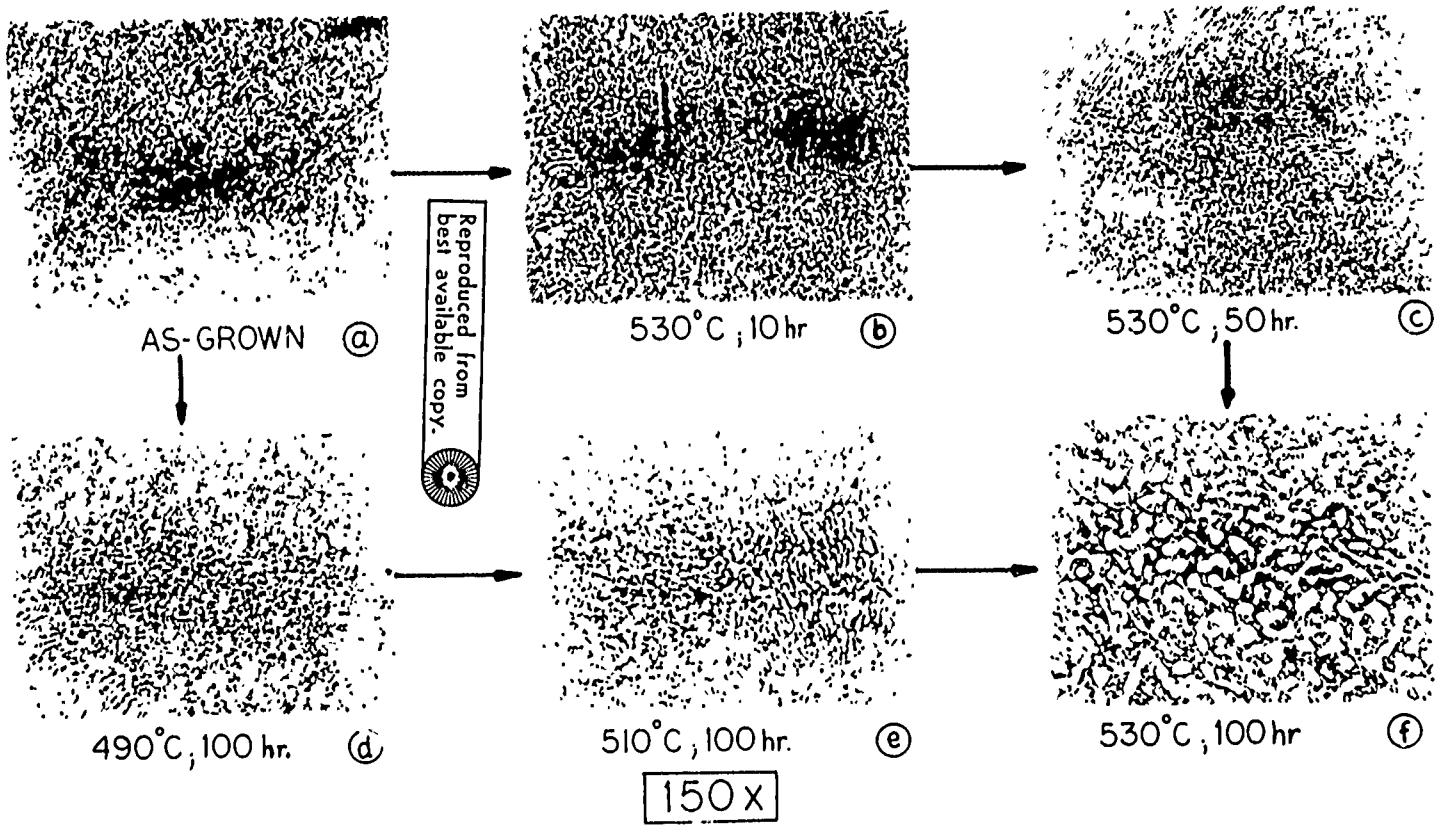

Figure 5

Microstructural changes in lamellar Al-$CuAl_2$ exposed at elevated temperatures; transverse sections; lighter phase is $CuAl_2$.

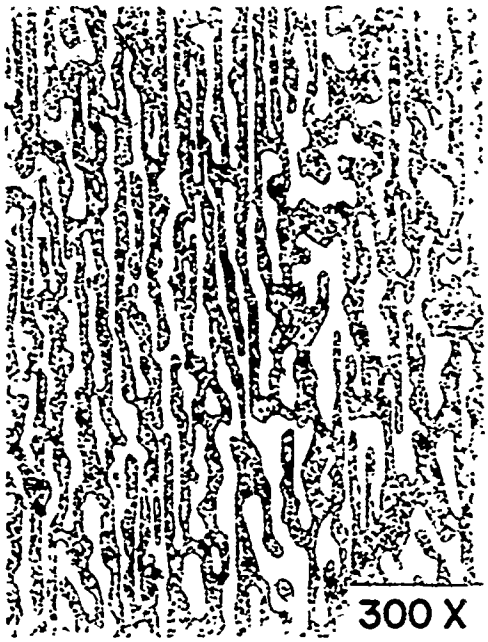

Figure 6

Microstructure of Al-$CuAl_2$ following exposure at 530°C for 100 hours; lighter phase is $CuAl_2$; longitudinal section.

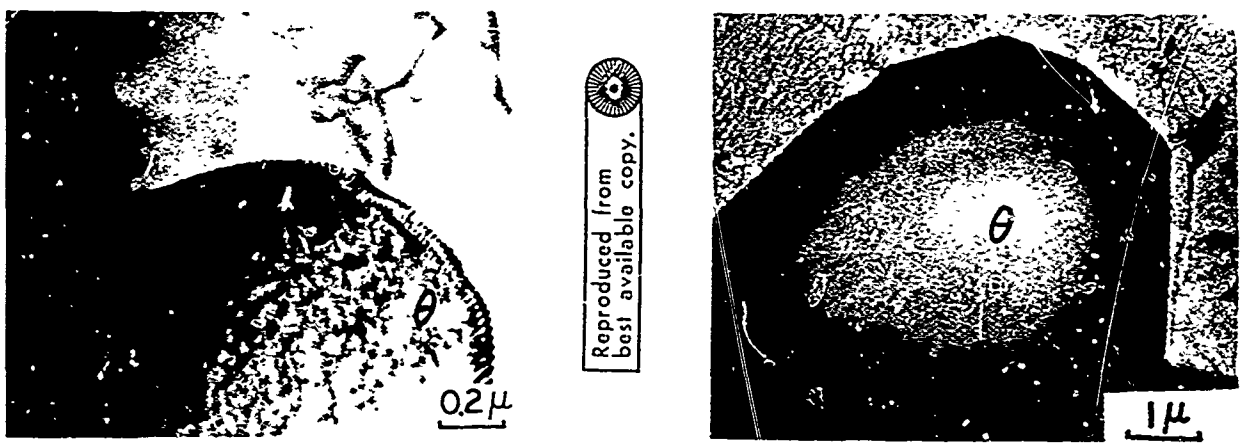

(a) (b)

Figure 8

TEM illustrating faceting of the $CuAl_2$ (θ) phase (a) transverse section, directionally solidified; (b) transverse section exposed 100 hours at 530°C.

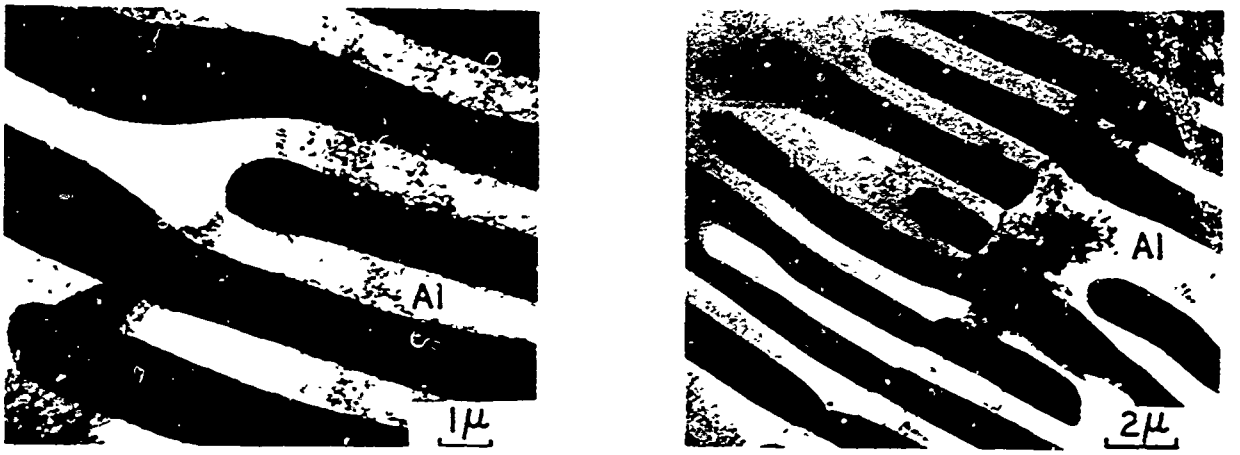

(a) (b)

(c)

Figure 7

TEM showing coarsening in Al-$CuAl_2$; transverse sections; (a) 10 hours at 530°C; (b) 10 hours at 530°C; (c) 100 hours at 530°C.

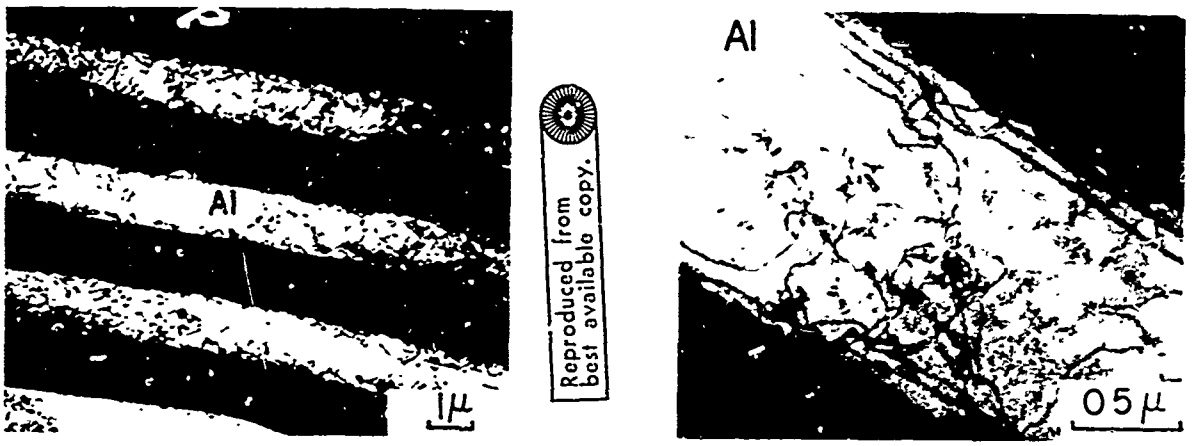

(a) (b)

Figure 9

TEM - Deformation substructure in Al-$CuAl_2$; directionally solidified condition; transverse sections.

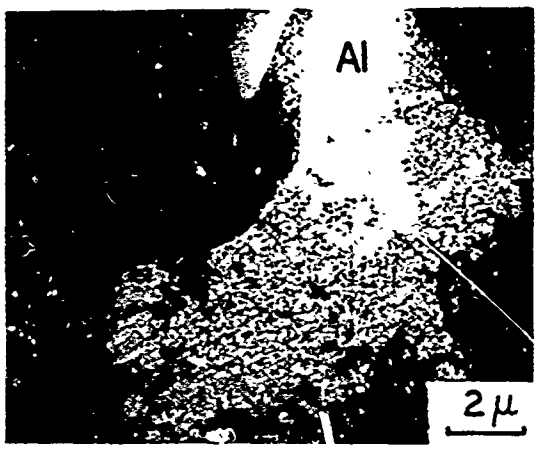

(a)

(b)

(c)

Figure 10

TEM - Deformation substructure in Al-$CuAl_2$ following elevated temperature exposure (100 hours at 530°C); transverse sections.

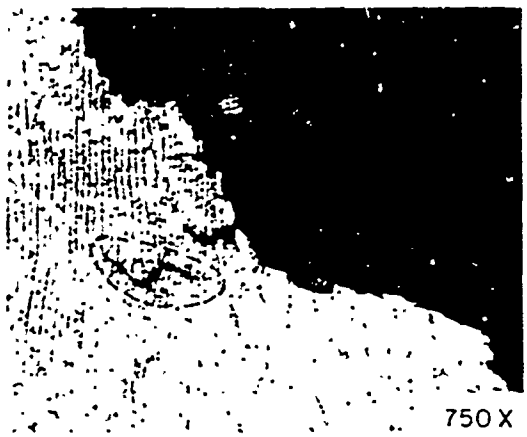

(a)

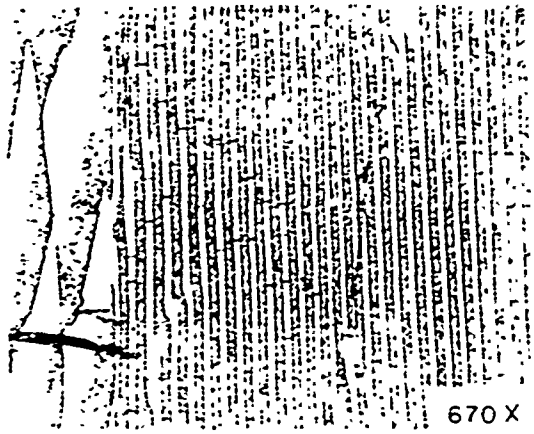

(b)

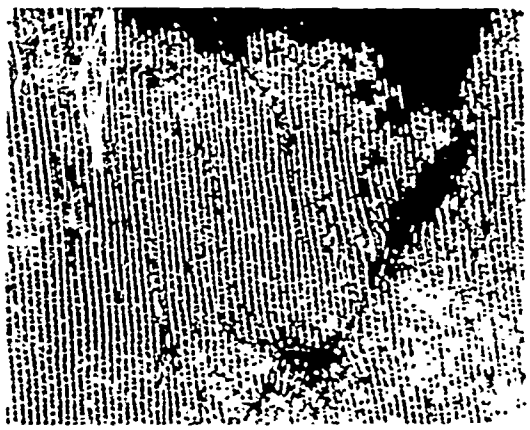

(c)

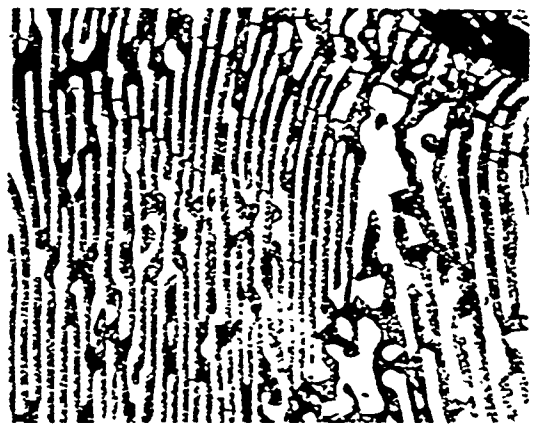

(d)

Figure 11

Longitudinal sections close to the fracture surface of Al-$CuAl_2$: (a) and (b) directionally solidified condition; (c) 100 hours at 490°C; (d) 100 hours at 530°C.

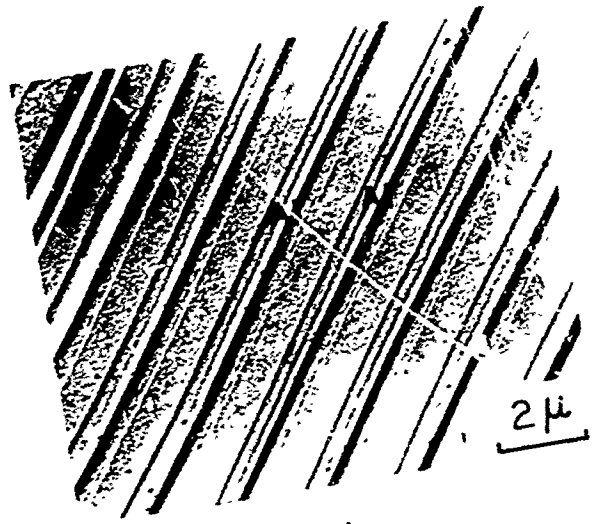

(a)

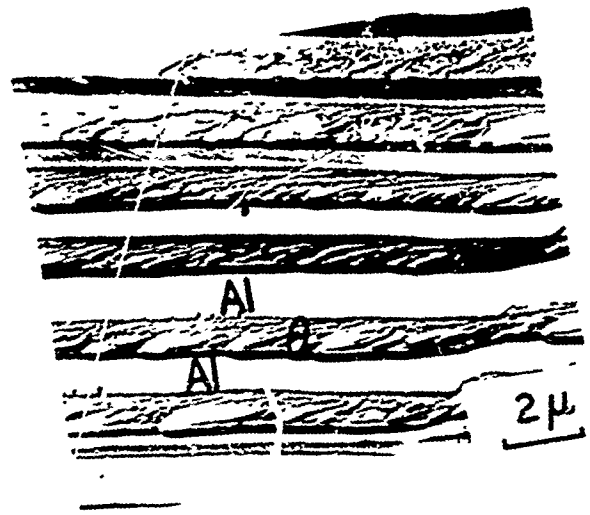

(b)

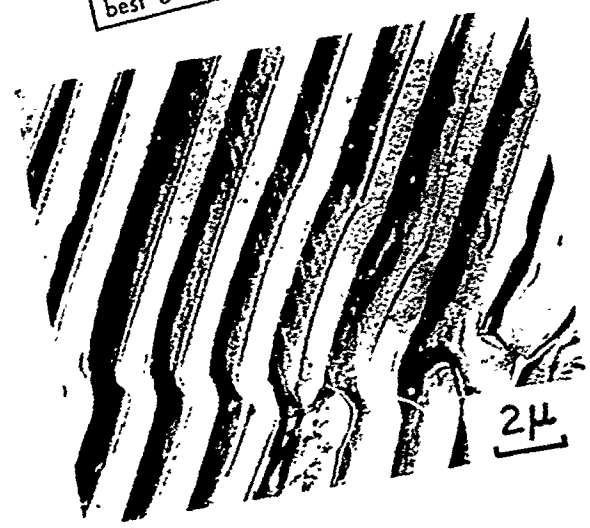

(c)

Figure 12

Electron fractographs of Al-$CuAl_2$ in the directionally solidified condition; tensile failure.